Time-resolved atomic force microscopy imaging studies of asymmetric PS-b-PMMA ultrathin films: Dislocation and disclination transformations, defect mobility, and evolution of nanoscale morphology

J. Hahm and S. J. Sibener[a)]
The James Franck Institute and Department of Chemistry, The University of Chicago, 5640 South Ellis Avenue, Chicago, Illinois 60637

(Received 9 May 2000; accepted 29 November 2000)

Time-sequenced atomic force microscopy (AFM) studies of ultrathin films of cylinder-forming polystyrene-block-polymethylmethacrylate (PS-b-PMMA) copolymer are presented which delineate thin film mobility kinetics and the morphological changes which occur in microphase-separated films as a function of annealing temperature. Of particular interest are defect mobilities in the single layer (L thick) region, as well as the interfacial morphological changes which occur between L thick and adjacent $3L/2$ thick layers, i.e., structural changes which occur during multilayer evolution. These measurements have revealed the dominant pathways by which disclinations and dislocations transform, annihilate, and topologically evolve during thermal annealing of such films. Mathematical combining equations are given to better explain such defect transformations and show the topological outcomes which result from defect–defect encounters. We also report a collective, Arrhenius-type flow of defects in localized L thick regions of the film; these are characterized by an activation energy of 377 kJ/mol. These measurements represent the first direct investigation of time-lapse interfacial morphological changes including associated defect evolution pathways for polymeric ultrathin films. Such observations will facilitate a more thorough and predictive understanding of diblock copolymer thin film dynamics, which in turn will further enable the utilization of these nanoscale phase-separated materials in a range of physical and chemical applications. © *2001 American Institute of Physics.* [DOI: 10.1063/1.1342239]

I. INTRODUCTION

The behavior of polymer thin films at surfaces and interfaces is of considerable interest because of the immense technological promise such films hold for high performance materials and devices.[1] Polymer thin films exhibit distinct structural, optical, mechanical, and thermal properties from their bulk counterparts due to the presence of strong substrate interactions and associated confinement in low dimensions. One aspect of this paper will deal with defect mobility kinetics in thin films and the morphological changes of diblock copolymer ultrathin films which occur in microphase-separated films as a function of annealing temperature. Another aspect will be to delineate defect dynamics involving dislocation and disclination transformations in such films. Before discussing the relevant behavior of these complex systems, we will begin by briefly reviewing previous studies involving simpler systems, such as homopolymers or blends.

In the case of homopolymers, previous studies have reported modified thermal or mechanical properties near underlying substrates.[2–5] For example, large changes in the thermal expansion characteristics of poly(2-vinyl pyridine) films supported on acid-cleaned silicon oxide substrates have been demonstrated.[2] The presence of surfaces can alter polymer dynamics by inhibiting polymer chain mobility.[3–5] Moreover, it is not yet precisely known how surface interactions influence microphase separation and related microstructural changes which are unique to thin films. Some studies have begun to address these issues,[3–5] e.g., E. K. Lin *et al.* have measured slower interdiffusion of poly(methyl methacrylate) chains on silicon oxide substrates with decreasing film thickness using neutron reflectometry.[3] By systematically varying substrates from silicon oxide to silicon hydride to poly(2-vinylpyridine), Zheng *et al.* have observed monomer friction coefficients for each of these polystyrene-surface systems which are greater than the respective bulk melt values.[4] A substantial decrease in the lateral diffusion of polystyrene chains on silicon oxide substrates has been observed in films thinner than 1500 Å.[5]

Diblock copolymer dynamics near interfaces and surfaces are not as well understood as those characteristic of homopolymers and blends.[2–6] Self-diffusion in block copolymer thin films is complicated due to the inherent anisotropy of the copolymer motion. The dynamics of microphase-separated diblock copolymers are governed by thermodynamic penalties for segment contacts, mechanisms for center of mass mobility, and the temperature dependent monomeric friction dependence between the two blocks.[7] Hamersky *et al.* have studied self-diffusion of poly(ethylene oxide-b-ethylethylene) diblock copolymer, PEO-b-PEE, in the gyroid and cylinder phases using forced Rayleigh scattering (FRS) and nuclear magnetic resonance (NMR).[7] They observed faster polymer mobility along the cylinders than across the

a)Author to whom correspondence should be addressed. Electronic mail: s-sibener@uchicago.edu

cylinders due to the greater thermodynamic penalty associated with diffusion across the cylinders. Similar phenomena were reported for symmetrical poly(ethylenepropylene)-poly(ethylene) diblock copolymers near their order–disorder temperature, where diffusion along the lamellae occurred faster than across the lamellae.[8]

Another critical issue governing the properties of diblock copolymer films is the presence of topological defects. Defects play a crucial role in determining and limiting technologically useful properties of these materials. Detailed studies of the dynamics of defect evolution pathways in polymer thin films are currently lacking.

In this paper, we present a comprehensive study of the statistics and dynamics of topological defects in polymeric thin films. The types and configurations of defects which are commonly observed in diblock copolymer systems are very similar to those found in liquid crystal systems where the defects are well characterized.[9–11] Topological defects draw considerable interest because edge dislocations or disclinations, for example, cannot be eliminated by a simple continuous distortion of the surrounding molecular alignments.[10] The interactions of topological defects within a paired disclination, and among multiple disclination pairs, are in particular very intriguing. Previous attempts have been made to apply the knowledge gained from defect studies involving liquid crystals to defects in polymer systems. Amundson and co-workers utilized this analogy between smectic liquid crystals and symmetric diblock copolymer domains to characterize their polymeric system.[12–15] Similarly, Turner *et al.* have studied edge dislocations in PS-b-PMMA lamellar films,[16] while defects in mixed lamellar PS-b-PMMA films have also been investigated using this methodology.[17] Despite the difficulties that arise from the differences between polymeric systems and liquid crystalline systems, the polymer–liquid crystal analogy has also been successfully used to study distortions in polymer microdomains resulting from the existence of defects.[18]

To understand the interaction between topological defects, monitoring defect transformation in real-time is highly desirable. Tracking such defect evolution was not easily obtainable until recently due to the limitations of the techniques typically used to study defects in polymer films, such as high resolution electron microscopy (HREM) and transmission electron microscopy (TEM).[19–21] Other traditional techniques used to study polymer dynamics including scattering techniques,[22–24] forward recoil spectrometry (FRES),[8] and secondary ion mass spectrometry (SIMS)[3,4] have other complications. For example, to monitor diffusion behavior, tagging of polymer chains with isotopes is required for FRES and SIMS. Despite the best efforts with these methods, much of the desired details on the dynamics of individual domains have not been obtained. What is clearly needed is a straightforward way to repeatedly observe the dynamics of individual domains, and the associated interfacial morphological changes, noninvasively, on the nanometer scale.

Atomic force microscopy (AFM) meets these critical requirements. It has been previously used to study a variety of polymeric materials such as polymer single crystals, liquid crystals, and biopolymers.[25] In our previous Communication, we employed this technique to track an individual microdomain of PS-b-PMMA between repeated annealing treatments.[26] In this paper, we systematically extend these AFM studies to obtain mobilities of cylinder-forming PS-b-PMMA thin films on a silicon nitride substrate. This is accomplished by tracking individual topological defects and associated interfacial motion. We herein report the first direct investigation of interfacial morphological change related to such polymer motion. We have previously reported changes of local defect structure resulting from thermal annealing, focusing on local structural changes in PS-b-PMMA microdomains,[26] demonstrating how microdomains relink and join to reduce the total number of defects, or to acquire energetically more stable forms to minimize polymer chain stretch or compression. We have also described the high degree of microdomain alignment that can occur spontaneously during the formation of annular structures.[27] In the present study, we significantly extend our prior examination of topological defect interactions, especially interactions between paired disclinations. For the first time, we explicitly track multiple steps involved in defect annihilation and propagation, and explain mathematical transformation steps which lead to the topological outcome extracted from close examination of recurring disclination pairs.

II. EXPERIMENT

Asymmetric PS-b-PMMA (molecular weight 84 000 amu) was obtained from Polysciences, Inc (Warrington, PA). The diblock contained 75% PS by weight with a polydispersity of 1.08. The diblock sample was Soxhlet extracted with cyclohexane to remove excess PS homopolymer. Diblock thin films were prepared via spin casting onto a Si_3N_4 substrate at 3500 rpm for 1 min. The sample was then subsequently annealed in an argon atmosphere at various temperatures above its glass temperature, 375 K. Annealing temperatures ranged from 513 K to 528 K, with a chosen temperature held constant to within 1 K. The annealing temperature was preceded by a transient ramp-up rate of 5 K/min from room temperature, and quenched back to room temperature with a cooling rate of 2 K/min. The average film thickness measured by ellipsometry was 50 nm. The substrate contained transparent $60\,\mu m \times 60\,\mu m$ membranes patterned by using methods such as chemical vapor deposition, electron beam lithography, and anisotropic chemical etching. Detailed procedures for preparing this patterned substrate have been described elsewhere.[28] Time-sequenced AFM measurements were then conducted to examine the mobility and the interfacial morphology change of the diblock. Patterned membranes on the substrate allowed tracking of an individual domain between annealing cycles, i.e., all AFM imaging was done at room temperature following *ex situ* annealing treatments of the sample. AFM measurements were carried out using a Topometrix Discover; noncontact AFM imaging was performed with a silicon probe tip, while contact mode scanning was done using a silicon nitride probe with an applied force of 1 nN.

PMMA favors the silicon nitride substrate because of its lower wetting energy.[28] At the polymer/air interface, the sur-

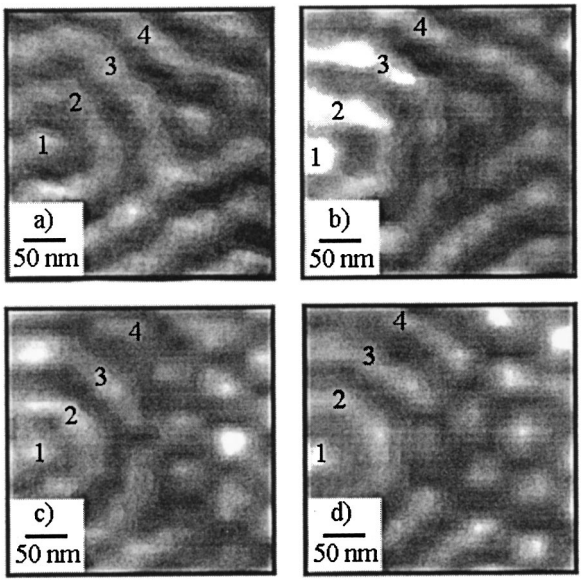

FIG. 1. Time lapse AFM images, 300 nm×300 nm, showing the interfacial morphological transformation of *parallel* cylinders to *vertical* cylinders at the boundary film region between L and advancing $3L/2$ thick layers after sequential annealing treatments (523 K, 1 h duration). PMMA (bright) microdomains in each image are numbered to easily identify them.

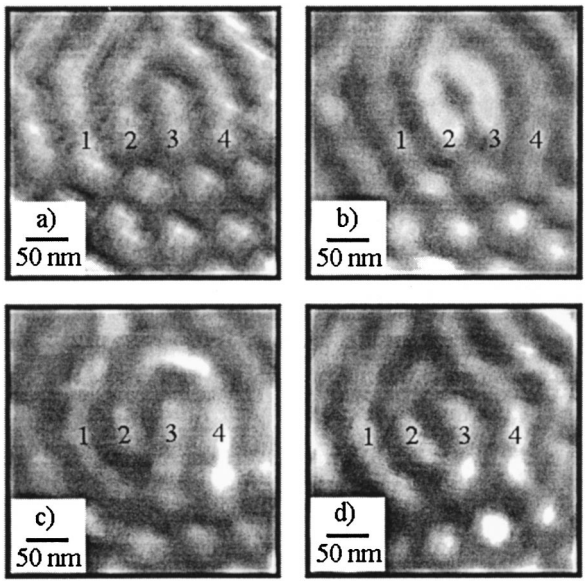

FIG. 2. Time lapse AFM images, 300 nm×300 nm, showing the interfacial morphological transformation of *vertical* cylinders to *parallel* cylinders at the boundary film region between L and retracting $3L/2$ thick layers after sequential annealing treatments (523 K, 1 h duration). PMMA (bright) microdomains in each image are numbered to easily identify them.

face tension difference between PMMA and PS is small enough to produce the appearance of both components at the upper interface of certain film areas when the film is prepared as described above.[28] The film areas with both components exposed are herein referred to as ''L thick'' regions, where L is 43 nm.[26] This was determined by combined TEM and AFM imaging of the same film location.[28] The PS-b-PMMA diblock copolymer forms one layer of lying-down cylindrical microdomains parallel to the substrate, *parallel cylinders*, in the L thick layer.[28] These regions yield AFM topographical contrast of 1 nm where PMMA is higher than PS.[28] The average cylinder spacing in the L thick region, measured by both TEM and AFM, is 50 nm.[26]

III. RESULTS AND DISCUSSION

This section is divided into five parts. (A) Interfacial morphology changes between the L thick and neighboring $3L/2$ thick film areas; (B) dynamics of topological defects and mobilities associated with the evolution of the multilayers where collective defect flow is observed; (C) classification of topological defects in PS-b-PMMA ultrathin films including relevant background material; (D) topological characterization of defect–defect interactions and outcomes; and (E) preliminary attempts to observe the intermediate structural transition states which mediate the approach to lowest-energy microdomain configurations.

A. Interfacial morphology change

We observe that thermal annealing induces morphological changes at the interface between the L thick and the neighboring $3L/2$ thick region. Time-lapse AFM images in Figs. 1 and 2 are taken consecutively from the same film location after repeated annealing treatments at 523 K. The morphological transformations between cylinders oriented parallel to the underlying substrate (*parallel cylinders*) and cylinders oriented perpendicular to the substrate (*vertical cylinders*), Fig. 1, and vice versa, Fig. 2, at the interface are clearly resolved in the AFM images. Such interfacial changes are directly linked to the expansion and contraction of L thick regions. Morphological changes between vertical and parallel cylinders are associated with polymer film thickness changes induced by thermal annealing treatments.[29] Suh *et al.* predicted such transformations between vertical and parallel morphologies in cylindrical block copolymer domains when the difference in the surface tension between two polymer components of the block is sufficiently small, and when the film thickness is less than a few repeat spacings.[29] This delicate energetic balance is observed in our experiments.

The expansion and contraction of symmetric films such as PS-b-PMMA[30] and poly(styrene)-poly(butylmethacrylate)[31] have been studied previously on surface depressions or elevations which represent areas of different film thicknesses using *in situ* interference microscopy. The growth mechanisms of these two-dimensional domains[31] include expansion and contraction of a domain, coalescence of neighboring domains, and the disappearance of smaller domains for the benefit of larger domains, i.e., Ostwald ripening.[32] Time resolved AFM images of the asymmetric PS-b-PMMA in Fig. 3 illustrate the evolution of L thick domains where contraction of L thick regions (dark areas in the AFM images) dominates. Also seen is the disappearance of L thick regions as they convert to $3L/2$ thick domains.

B. Collective defect flow and mobility

We now report polymer defect mobility results obtained by examining consecutive AFM images. Such sequences can

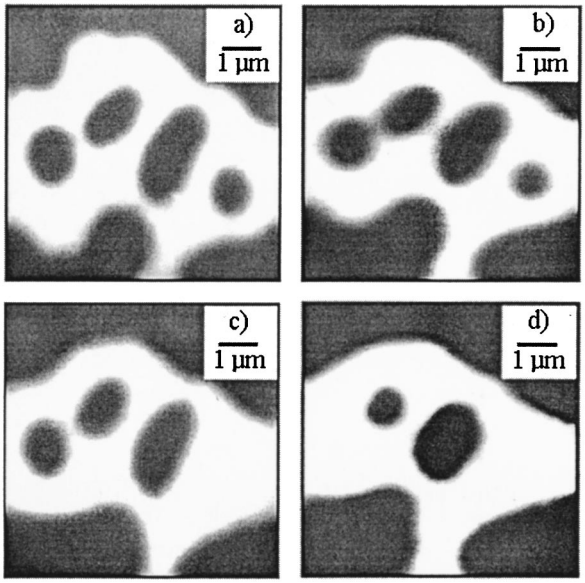

FIG. 3. Time lapse AFM images, 7 μm$\times$7 μm, showing L and $3L/2$ thick regions between sequential annealing treatments (513 K, 12 h duration). Bright and dark regions are $3L/2$ and L thick film areas, respectively. Several of the initially present L thick regions disappear during annealing.

provide information on polymer motion, such as flow patterns, velocities, and activation energies under various annealing treatments. Of particular interest is defect mobility within cylindrical microdomains in L thick regions. This is examined between 513–528 K. Annealing times in these experiments vary due to strong temperature dependence of the polymer chain mobility. The 513 K and 516 K data sets were annealed for 3 h while the 523 K and 528 K data needed only 1 h. The annealing cycles were repeated at least four times for each of these temperatures. These annealing conditions were chosen to allow significant measurable defect motion by post-AFM imaging. Figure 4(A) shows defect motion monitored before and after an hour of annealing at 523 K. Relative positions of defects in sequential images were determined using at least two fixed reference points on the substrate. We track defects in a given region and record the initial (bottom of the arrows) and final (top of the arrows) coordinates of nonannihilating defects between annealing treatments. We then extract flow patterns and velocities of the defect motion in the given area of the film at a chosen temperature. Various types of defects exist in the polymer film, and their mobilities can differ between defect types. Further investigations are underway to precisely correlate defect types with their corresponding translational activation energies. The defect velocities that we obtained in the experiment were averaged over time and all defect types in a chosen area, bigger than 2 μm$\times$2 μm, yielding an average defect density of about 20 per 1 μm^2. We observe a collective defect flow in this L thick domain as shown in Fig. 4. Such collective dynamics implies that defect motion is highly correlated. We hypothesize that this coherent defect motion may come from the heterogeneity in the film thickness which can be produced by, for example, the interaction between neighboring domains as displayed in Fig. 3. This interaction results in expansion or contraction of a given domain, thereby

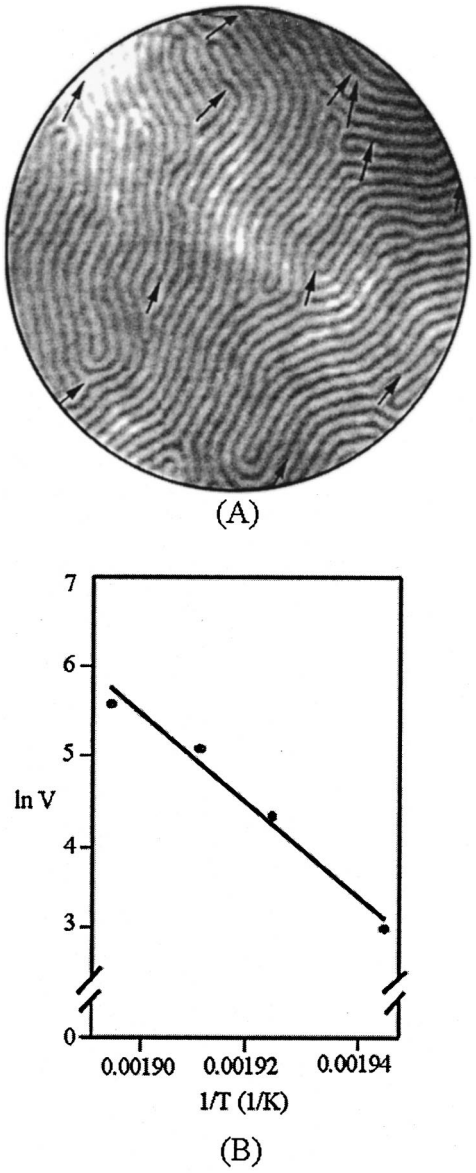

FIG. 4. (A) AFM image, 2 μm in diameter, showing coherent defect motion (arrows) in PS-b-PMMA microdomains following 1 h of annealing at 523 K. See text for positional referencing of sequential images. (B) A plot of $\ln(V)$ vs $1/T$ displaying Arrhenius behavior for defect motion with an activation energy of 377 kJ/mol, V is the defect velocity, and T is the temperature.

causing changes in the local film thickness and also possibly introducing film regions that are not completely height-quantized. Thermal annealing will induce coherent polymer chain motion in order to minimize film regions of nonequilibrium thicknesses. Within an L thick domain, defects interact with one another through stress fields produced by the necessary stretch or compression of polymer chains around their cores.[10]

Mobilities of polymers change as a function of annealing temperature. In bulk samples, self-diffusion of a diblock copolymer is determined by viscous drag between polymer chains. The viscosity is governed by the Williams, Landel and Ferry (WLF) temperature dependence.[33] They found that

a temperature shift factor, a_T, can be obtained using the formula,

$$\log_{10} a_T \cong -17.44(T-T_g)/(51.6+T-T_g),$$

where T_g is the glass transition temperature of the material. This equation predicts much slower polymer chain motion when the annealing temperature is closer to its glass transition temperature. The average velocities of defect motions are 21 nm/h at 513 K, 74 nm/h at 516 K, 158 nm/h at 523 K, and 261 nm/h at 528 K (with a standard deviation of 10 nm/h). We note that, within the limited temperature range of our experiment, the defect motion also displays Arrhenius behavior. By plotting the measured velocities (V) as a function of temperature (T), $\ln(V)$ vs $1/T$, the activation energy of the collective and averaged defect mobility is determined to be 377 kJ/mol of Fig. 4(B). Defect motion in L thick regions cannot be identified with diffusion of a specific microdomain. However, significant information on polymer chain mobility and its temperature dependence in thin films is reflected on the relinking and joining processes of the microdomains which result in defect annihilation and propagation.

Friedman and Porter have developed a semiempirical mixing rule for mixtures of homopolymer samples which was used to fit the viscosity data for PS-b-PMMA block copolymer bulk samples.[33–35] They obtained an activation energy of 122 kJ/mol for PS-b-PMMA bulk samples where the volume fraction of PS was 75% and the average molecular weight of the diblock was 91 000 amu. In our indirect measurement on PS-b-PMMA chain mobility, we observe much slower mobility and about threefold higher activation energy in the ultrathin layer regions. This significant difference between thin film and bulk behavior likely comes from the presence of the underlying substrate.

C. Topological defects in PS-b-PMMA thin films

Topological defects in polymer thin films exhibit configurations which are related to those commonly observed in liquid crystalline systems. Drawing on the extensive literature for such defects in liquid crystals,[9,11,36–41] we herein extend such ideas to the examination of topological defects in polymer thin films. Defects in ultrathin (single layer thick) polymer films are confined within a two-dimensional surface. Therefore, distortions in such polymer thin films come from splay and bend distortions. These distortions limit the degree of orientational order, while the translational order of the microphase separated polymer remains fixed at 50 nm.

Edge dislocations are frequently observed in diblock copolymer thin films. In liquid crystalline systems, these dislocations are classified by analyzing changes in a director rotation around a dislocation core.[9] A director **n** is a vector which represents the direction of the average molecular alignment. In an actual physical situation, the director exhibits various discontinuities in inclination resulting in disclinations. Microdomains in diblock copolymer films, resulting from the microphase separation of two polymer components of the diblock, can be viewed as alternating layers of polymer segments in a two-dimensional surface. Edge dislocations in polymer thin films can therefore be categorized according to their signs and strengths via this polymer–liquid crystal analogy. Plus and minus disclinations with a strength of $\frac{1}{2}$ are commonly observed in diblock copolymer domains due to the physical identity of **n** and $-$**n**. To distinguish disclination cores consisting of the two components of the diblock, we hereafter label disclination cores consisting of either PMMA and PS with ''pmma'' and ''ps,'' respectively, as subscripts. Disclinations with opposite signs usually emerge as pairs. Examples of dislocations and paired disclination lines in this asymmetric diblock are shown in Fig. 5.

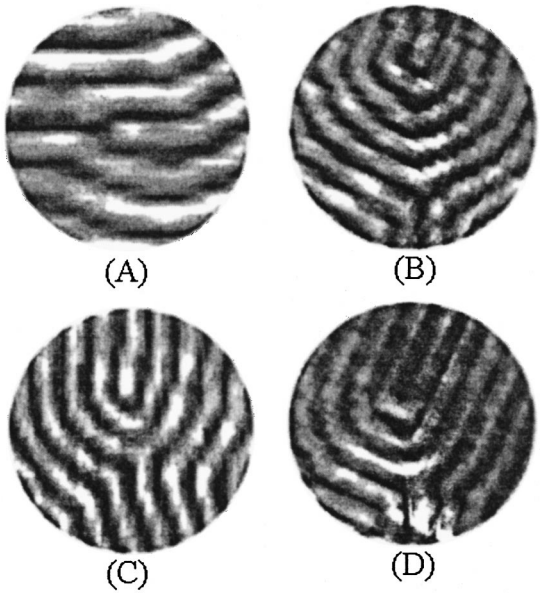

FIG. 5. Examples of topological defects which are commonly observed in single layer thick cylinder-forming PS-b-PMMA films. The repeat spacing of the cylinders is 50 nm, and the average corrugation of the alternating cylinders is 1 nm. (A) A dislocation of pmma, (B) a disclination pair: (+1/2)pmma and (−1/2)ps, (C) a disclination pair: (+1/2)pmma and (−1/2)pmma, and (D) a disclination pair: (+1/2)ps and (−1/2)pmma.

D. Topological defect transformations

We now systematically investigate topological defect interactions and discuss transformation mechanisms within and between defect pairs. Such transformations can be grouped into four categories: (1) interactions between +1/2 and −1/2 disclinations, (2) interactions between + and − dislocations, (3) interactions between disclination pairs, and (4) interactions between dislocations and disclinations. Topological interactions categorized in this manner are frequently observed in our AFM investigation, as summarized in Tables I and II and related text.

1. Interactions between +1/2 and −1/2 disclinations

Interactions between +1/2 and −1/2 disclinations can be subcategorized into two cases depending on the core types and signs of the interacting disclinations. These cases can produce ''stable'' (propagating) or ''unstable'' (annihilating) sets of defect pairs depending on their local environment.

a. Annihilating disclinations. Two disclinations of the same core type but with opposite signs will interact and annihilate when they propagate to the distance of one repeat spacing apart from each other, cases [1] and [3] of Tables I

TABLE I. Topological combining cases for allowed defect transformations.

A. *Interactions between +1/2 and −1/2 disclinations* (4 cases)
[1] (+1/2)pmma+(−1/2)pmma→no defect
[2] (+1/2)pmma+(−1/2)ps↔(+1/2)ps+(−1/2)pmma
[3] (+1/2)ps+(−1/2)ps→no defect
[4] (+1/2)ps+(−1/2)pmma↔(+1/2)pmma+(−1/2)ps
B. *Interactions between + and − dislocations* (4 cases)
[5] (+Dislocation)pmma+(−dislocation)pmma→no defect
[6] (+Dislocation)pmma+(−Dislocation)ps→no defect
[7] (+Dislocation)ps+(−dislocation)ps→no defect
[8] (+Dislocation)ps+(−dislocation)pmma→no defect
C. *Interactions between disclination pairs* (10 cases)
[9]{(+1/2)pmma+(−1/2)pmma}+{(+1/2)pmma+(−1/2)pmma}→no defect
[10] {(+1/2)pmma+(−1/2)pmma}+{(+1/2)pmma+(−1/2)ps}↔(+dislocation)pmma or {(+1/2)pmma+(−1/2)ps}
[11] {(+1/2)pmma+(−1/2)pmma}+{(+1/2)ps+(−1/2)ps}→no defect
[12] {(+1/2)pmma+(−1/2)pmma}+{(+1/2)ps+(−1/2)pmma}↔(−dislocation)pmma or {(+1/2)pmma+(−1/2)ps}
[13] {(+1/2)pmma+(−1/2)ps}+{(+1/2)pmma+(−1/2)ps}→no defect
[14] {(+1/2)pmma+(−1/2)ps}+{(+1/2)ps+(−1/2)ps}↔(+dislocation)pmma or {(+1/2)pmma+(−1/2)ps}
[15] {(+1/2)pmma+(−1/2)ps}+{(+1/2)ps+(−1/2)pmma}→no defect
[16] {(+1/2)ps+(−1/2)ps}+{(+1/2)ps+(−1/2)ps}→no defect
[17] {(+1/2)ps+(−1/2)ps}+{(+1/2)ps+(−1/2)pmma}↔(−dislocation)pmma or {(+1/2)pmma+(−1/2)ps}
[18] {(+1/2)ps+(−1/2)pmma}+{(+1/2)ps+(−1/2)pmma}→no defect
D. *Interactions between dislocations and disclinations* (16 cases)
[19] (+1/2)pmma+(+dislocation)pmma↔(+1/2)ps
[20] (+1/2)pmma+(−dislocation)pmma↔(+1/2)ps
[21] (+1/2)pmma+(+dislocation)ps↔(+1/2)ps
[22] (+1/2)pmma+(−dislocation)ps↔(+1/2)ps
[23] (−1/2)pmma+(+dislocation)pmma↔(−1/2)ps
[24] (−1/2)pmma+(−dislocation)pmma↔(−1/2)ps
[25] (−1/2)pmma+(+dislocation)ps↔(−1/2)ps
[26] (−1/2)pmma+(−dislocation)ps↔(−1/2)ps
[27] (+1/2)ps+(+dislocation)pmma↔(+1/2)pmma
[28] (+1/2)ps+(−dislocation)pmma↔(+1/2)pmma
[29] (+1/2)ps+(+dislocation)ps↔(+1/2)pmma
[30] (+1/2)ps+(−dislocation)ps↔(+1/2)pmma
[31] (−1/2)ps+(+dislocation)pmma↔(−1/2)pmma
[32] (−1/2)ps+(−dislocation)pmma↔(−1/2)pmma
[33] (−1/2)ps+(+dislocation)ps↔(−1/2)pmma
[34] (−1/2)ps+(−dislocation)ps↔(−1/2)pmma

and II. This annihilation interaction is represented in Equation (1), where → indicates that the forward direction is favored in the thermal annealing experiment,

$$(+1/2)\text{pmma,ps}+(-1/2)\text{pmma,ps}\rightarrow\text{No defect.} \qquad (1)$$

This transformation process is not typically energetically favorable, since the evolution of a disclination pair of the same type but of opposite signs has to generate dislocations to propagate. Indeed, we rarely observed the two annihilation cases, [1] and [3]; these cases were observed *only* when two disclinations of the same type but of opposite signs were in immediate proximity, i.e., were located one repeat spacing away from each other.

b. Propagating disclinations. When two disclinations with opposite core types and signs are near each other, the outcome of the interaction involving alternation of disclination core type is frequently observed, i.e., the core type flips between ps and pmma, see cases [2] and [4] of Tables I and II. Alternating ±1/2 disclination cores between pmma and ps allows further propagation of disclinations via the consumption or creation of a dislocation. A disclination (+1/2)pmma,ps can change into (+1/2)ps,pmma after an annealing treatment through relinking of the disclination line with a neighboring microdomain. This core change between pmma and ps produces a dislocation in the relinking process of the microdomains. A similar process is observed between (−1/2)pmma,ps and (−1/2)ps,pmma disclinations. The reverse process also occurs; when a dislocation is located one repeat spacing apart from a (+1/2) disclination of pmma or ps, the dislocation can interact with the disclination resulting in a ''core type change'' of the (+1/2) disclination to ps or pmma. Interaction processes involving an alternation of ±1/2 disclination cores between pmma and ps are summarized in Eqs. (2) and (3), where ↔ in these equations repre-

TABLE II. Schematically presented combining cases for topological defect transformations.

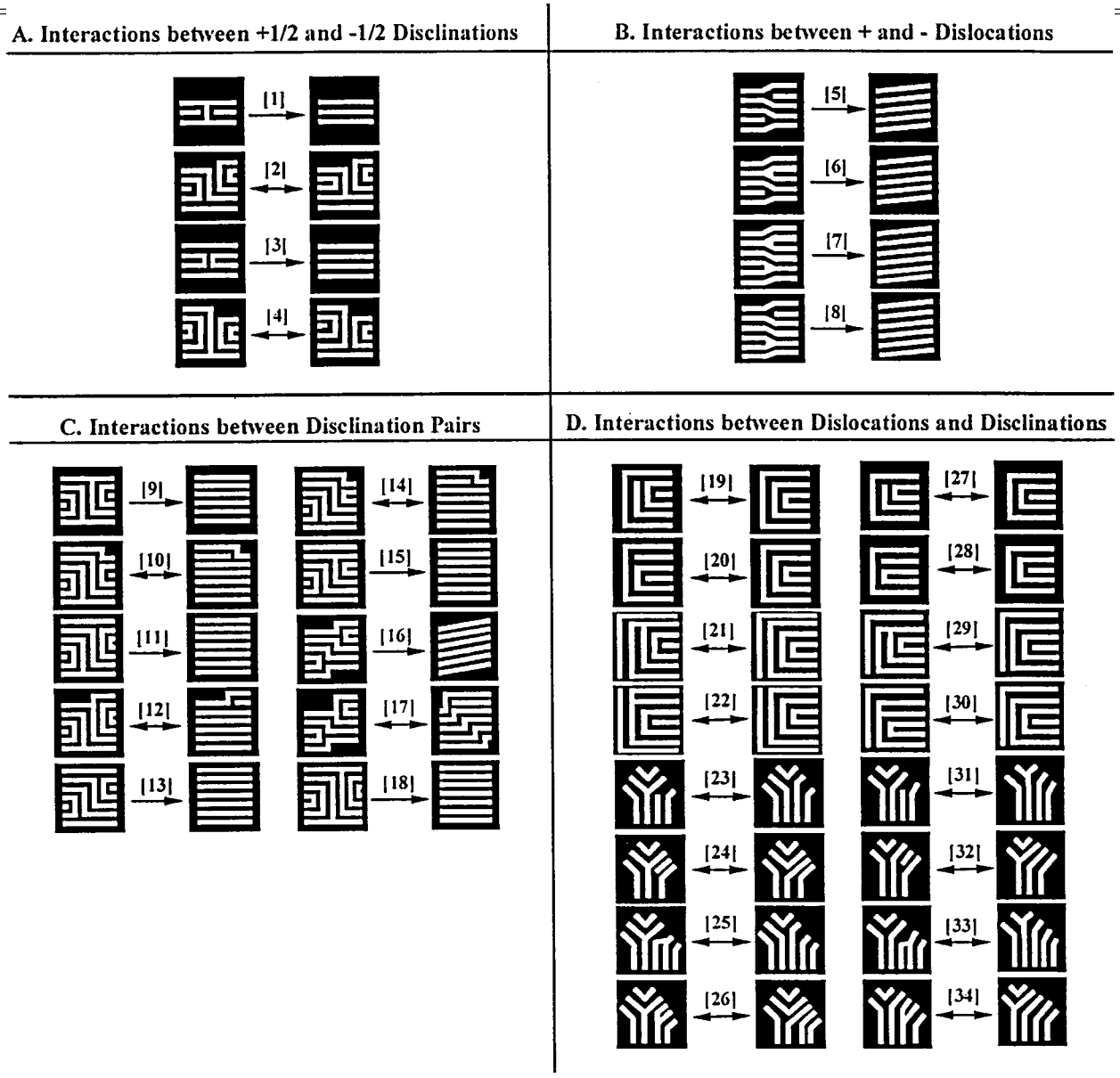

sents the reversible transformation of the disclination cores between annealing treatments,

$$(+1/2)\text{ps,pmma}+(+\text{dislocation})\text{pmma,ps} \leftrightarrow (+1/2)\text{pmma,ps}, \quad (2)$$

$$(-1/2)\text{ps,pmma}+(-\text{dislocation})\text{pmma,ps} \leftrightarrow (-1/2)\text{pmma,ps}. \quad (3)$$

The bias towards one process winning out over the other is strongly dependent on the local environment, such as types and signs of neighboring defects. We observe many examples where a disclination of pmma or ps changes its core type, generating a dislocation, which in turn can be used to interact with a neighboring disclination. Figure 6 clearly displays the interchange rules for the cores described by the two equations shown above. The interchange of defect core types becomes important when a paired disclination, $(+1/2)+(-1/2)$, is interacting with another paired disclination.

The interaction of two disclinations of opposite core types and signs, for example an interaction between $(+1/2)$pmma and $(-1/2)$ps, can be understood as a combination process of Eqs. (2) and (3). In this instance, two disclinations of different types, but with opposite signs, interact and result in their annihilation as well as formation of a dislocation via the core change process. Figure 7 displays such propagating interactions for a disclination pair of $(+1/2)$ps and $(-1/2)$pmma. Equation (4) is an example of a disclination pair interaction which results in the formation of another set of disclinations. These disclinations are stable, propagating defects which cannot be removed from the microdomains without interactions with other disclination pairs or dislocations,

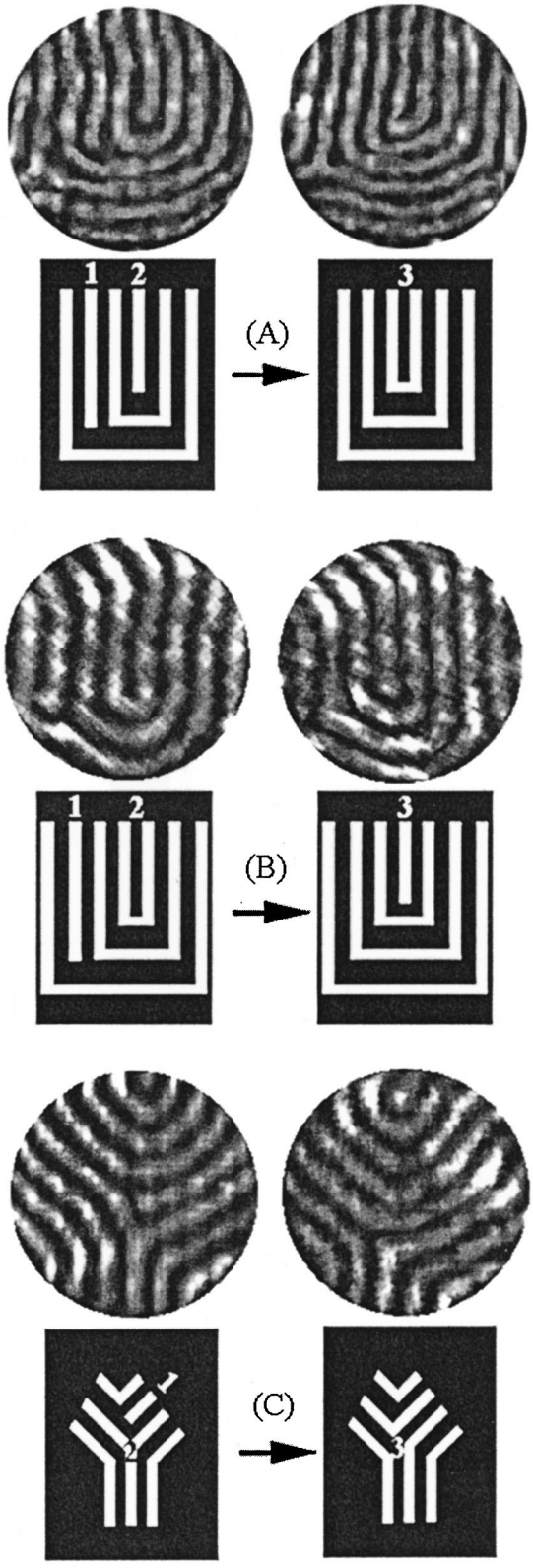

FIG. 6. AFM images taken before and after the polymer film is annealed for a further hour at 523 K where the repeat spacing of the cylinders is 50 nm. (A) A dislocation (marked as 1 in the schematic representation of the corresponding AFM image) interacts with a $(+1/2)$pmma disclination (marked as 2) to produce a $(+1/2)$ps disclination (marked as 3), see case [20]; (B) a dislocation (marked as 1) interacts with a $(+1/2)$ps disclination (marked as 2) to produce a $(+1/2)$pmma disclination (marked as 3), see case [28]; and (C) a $(-1/2)$pmma disclination (marked as 2) interacts with a dislocation (marked as 1) turns into a $(-1/2)$ps disclination (marked as 3), see case [24].

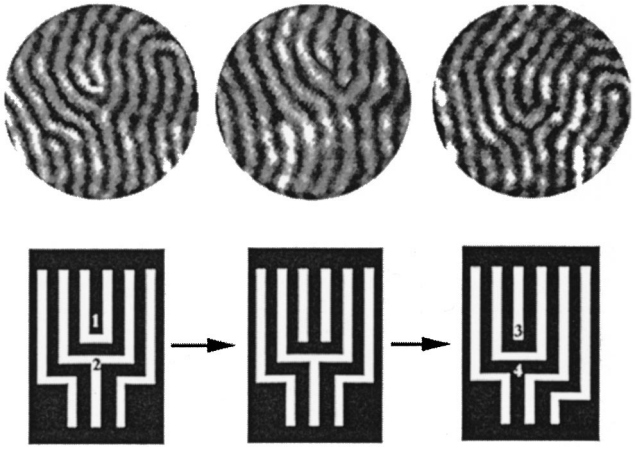

FIG. 7. AFM images taken between repeated annealing treatments of a further hour at 523 K showing an interaction described in case [4], involving a disclination pair of $(+1/2)$ps and $(-1/2)$pmma. In each image, the repeat spacing of the microdomains is 50 nm. $(+1/2)$ps and $(-1/2)$pmma disclinations are marked as 1 and 2, respectively, in the schematic representations which correspond to each AFM image. A series of images display how a disclination pair of $(+1/2)$ps and $(-1/2)$pmma changes into a disclination pair of $(+1/2)$pmma, marked as 3, and $(-1/2)$ps, marked as 4.

$$(+1/2)\text{pmma,ps}+(-1/2)\text{ps,pmma}$$
$$\leftrightarrow(+1/2)\text{ps,pmma}+(-1/2)\text{pmma,ps}. \quad (4)$$

Figure 8(A) displays images showing the evolution of two disclinations, $(+1/2)$pmma and $(-1/2)$ps. First, the $(+1/2)$pmma changes its core type to $(+1/2)$ps with the help of a nearby dislocation, producing $(+1/2)$ps and $(-1/2)$ps. The set of images in Fig. 8(B) demonstrates annihilation of these two disclinations, $(+1/2)$ps and $(-1/2)$ps.

2. Interactions between + and − dislocations

Interactions between + and − dislocations can be subcategorized depending on the types and signs of the interacting dislocations.

a Two dislocations of the same type but having opposite signs will interact and eventually annihilate when they propagate to within the distance of one repeat spacing. This interaction is schematically shown in cases [5] and [7] of Tables I and II,

$$(+\text{Dislocation})\text{pmma,ps}+(-\text{Dislocation})\text{pmma,ps}$$
$$\rightarrow\text{No defect}. \quad (5)$$

Two dislocations of the same core type but with opposite signs need to be one repeat spacing from each other for annihilation to occur. A dislocation embedded in the middle of highly aligned microdomains is harder to remove from the film due to its relatively immobile nature, i.e., a high energy cost is needed to reorient surrounding, stable polymer chains. However, a dislocation near a disclination is highly mobile, and plays a crucial role in defect annihilation and propagation.

b When two dislocations with opposite core types and signs are near each other, their configurations can be associated with a disclination of one sign and a dislocation of opposite sign. The combining rules for this case are de-

scribed in the previous paragraph regarding the alternation of disclination core types. The outcome of ''core flip'' processes of the two dislocations with opposite core types and signs is annihilation as given by cases [6] and [8] of Tables I and II.

3. Interactions between disclination pairs

Interactions between multiple disclination pairs are complicated, and depend strongly on the local distribution of defects. Ideal cases of isolated defect interactions with no effects from other nearby defect pairs are rare, partly because defects tend to segregate and cluster.[42] This is especially true in film regions near the interfaces between two neighboring domains. Finding isolated interacting defect pairs is therefore difficult. However, general insights on multiple disclination pair interactions can be extracted by analyzing local microdomain structural changes. The followings are some examples of such disclination pair interactions.

a. Annihilating disclination pairs:

$$\{(+1/2)\text{pmma,ps}+(-1/2)\text{ps,pmma}\}+\{(+1/2)\text{ps,pmma}+(-1/2)\text{pmma,ps}\}\rightarrow \text{No defect.} \tag{6}$$

In this case, (+1/2)pmma,ps of the first disclination pair annihilates with (−1/2)pmma,ps of the second disclination pair while (−1/2)ps, pmma of the first pair annihilates with (+1/2)ps,pmma of the second pair, see cases [15] and [18] of Tables I and II.

b. Propagating disclination pairs:

$$\{(+1/2)\text{pmma,ps}+(-1/2)\text{pmma,ps}\}+\{\underbrace{(+1/2)\text{ps,pmma}}_{\text{will be involved in core flip}}+(-1/2)\text{pmma,ps}\}\leftrightarrow,$$

$$\{(+1/2)\text{pmma,ps}+(-1/2)\text{pmma,ps}\}+\{\underbrace{(+1/2)\text{pmma,ps}+(+\text{Dislocation})\text{pmma,ps}}_{\text{the outcome of a core flip}}+(-1/2)\text{pmma,ps}\}\leftrightarrow$$

$$(+\text{dislocation})\text{pmma,ps}. \tag{7}$$

In this instance, (+1/2)pmma,ps of the first disclination pair can annihilate with (−1/2)pmma,ps of the second pair. However, (−1/2)pmma,ps of the first pair undergoes a core flipping process where the outcomes are (+1/2)pmma,ps + (+dislocation)pmma,ps. This resulting (+1/2)ps,pmma annihilates with (−1/2)pmma,ps while (+dislocation)pmma,ps propagates, see cases [19] and [20] of Tables I and II.

Other cases of permutated defect pair interactions can be predicted similarly using the combining examples shown as cases [9–18] given in Tables I and II. Figure 9(A) shows a series of images which display interaction processes for multiple disclination pairs after repeated annealing treatments. This sequence of AFM images is presented to demonstrate specific defect interaction processes such as ''core flip'' and annihilation where each step can be explained with corresponding mathematical rules, see figure captions. Defect interactions involving attraction between disclinations of opposite sign are seen in the series of images shown in Fig. 9(B). We observe, in many cases, that the core of a (−) disclination readily moves via constant connecting and disconnecting of nearby microdomains, while the core of a (+) disclination is less mobile. This faster mobility of (−) disclinations has been previously observed in the ±1/2 disclination mobilities of a polyester nematic phase.[43]

4. Interactions between dislocations and disclinations

Dislocations play a crucial role in the interactions of disclinations. This inseparable interaction process involving both dislocations and disclinations has been extensively discussed in the previous paragraphs concerning cases A, B, and C. The outcomes of all possible interactions between dislocations and disclinations are given by cases [19–34] of Tables I and II.

E. Relinking of microdomains

Topological defect interactions are driven by the stress fields associated with the extension or compression of polymer chains around disclinations or dislocations. We have observed an intermediate ''necking'' process that may originate from high stress fields around defects in the cylindrical domains. Figure 10(A) displays a series of AFM images showing the ''necking'' of a cylindrical domain in the vicinity of a defect, and the subsequent relaxation process to a reconfigured cylindrical domain after further annealing of the thin film. This process involves a series of steps; an existing cylinder balls up to first disconnect from the surrounding microdomain, then relinks, and finally relaxes to a modified cylindrical domain with a new configuration. This postulated relinking mechanism is shown schematically in Fig. 10(B). *In situ* variable temperature AFM measurements are needed to unravel the precise dynamics for this process.

IV. CONCLUSION

In this paper we have presented a comprehensive view of the topological changes and mobility kinetics for cylinder-forming PS-b-PMMA diblock copolymer thin films. Using

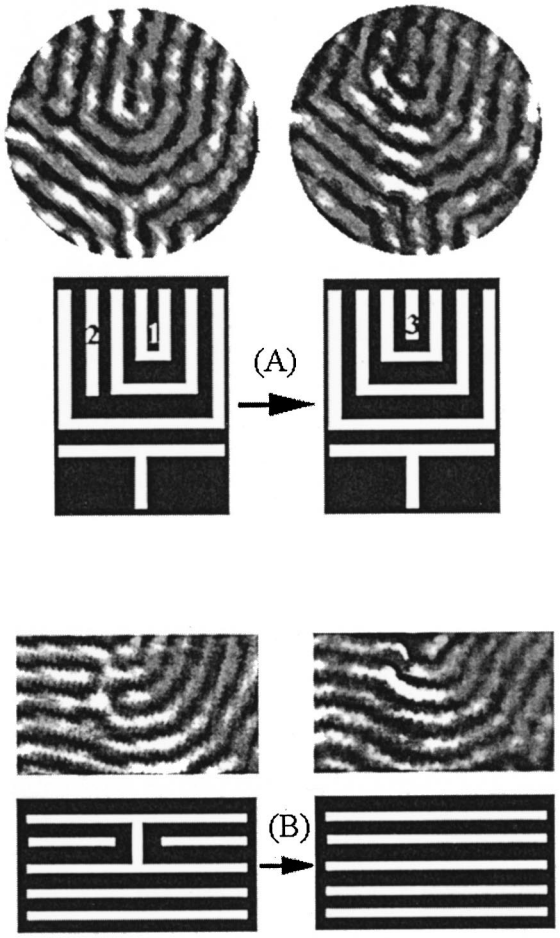

FIG. 8. (A) AFM images taken between repeated 1 h annealing treatments at 523 K showing an interaction involving a disclination pair of $(+1/2)$ps and $(-1/2)$pmma. In this case, the disclination of $(+1/2)$ps, which is marked as 1 in the schematic representation, interacts with a nearby dislocation (marked as 2) to change the core type to $(+1/2)$pmma marked as 3, see case [27]. This core change allows annihilation between $(+1/2)$pmma and $(-1/2)$pmma when the two disclinations propagate to the distance of one repeat spacing apart from each other as shown in (B). (B) Annihilation of two disclination pairs, i.e., 4 disclinations, where each pair consists of $(+1/2)$pmma and $(-1/2)$pmma disclinations, see case [9]. In each image, the repeat spacing of the microdomains is 50 nm.

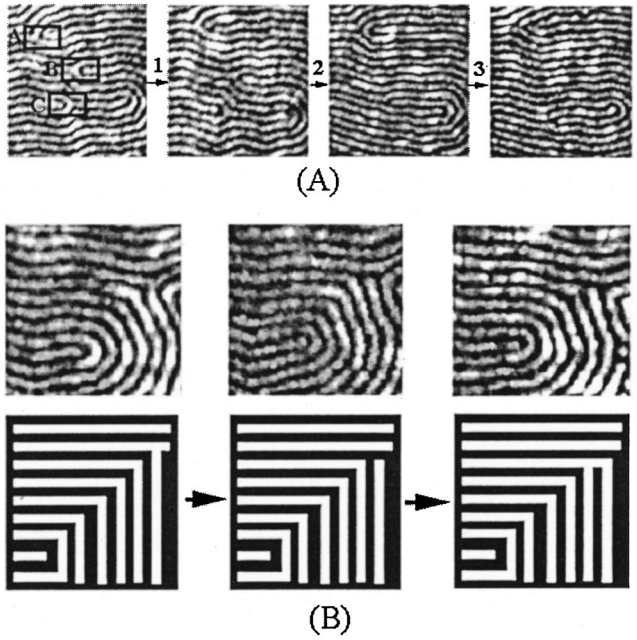

FIG. 9. (A) A series of AFM images taken between sequential 1 hour annealing treatments at 523 K which shows the evolution of three disclination pairs. Each pair is marked as A, B, and C in the first AFM image. Pairs A, B and C contain $(+1/2)$ps$+(-1/2)$pmma, $(+1/2)$pmma$+(-1/2)$pmma and $(+1/2)$pmma$+(-1/2)$pmma, respectively. Through interaction steps 2 and 3, pair A undergoes a ''core type change'' following case [4], leaving $(+1/2)$pmma$+(-1/2)$ps. The annihilation interaction of pairs B and C is completed after step 2, case [9]. Step 3 shows that pair A converts back to its original configuration via another core change process, case [4]. (B) Many examples, such as displayed in this figure, show that a minus disclination moves readily by relinking microdomains towards a plus disclination which is less mobile. In each image, the repeat spacing of the microdomains is 50 nm.

atomic force microscopy, we have sequentially imaged individual domains and defects as a function of thermal annealing conditions. These time-resolved studies have revealed fascinating aspects of the dynamics for these systems, such as the structural transformations that occur as multilayers evolve. We have also observed a collective, Arrhenius-type flow of the defects in localized *L*-thick regions of the film.

A major focus of this paper has been to examine the dynamics of defect–defect interactions. We have delineated the dominant pathways by which $(\pm 1/2)$ disclinations and dislocations interact, annihilate, and topologically evolve during thermal annealing. Mathematical combining equations are presented which classify such defect interactions, and which explain the topological changes which result from defect–defect encounters. For example, we have monitored interactions within and between disclination pairs, and given the combining mechanisms which present the possible topological outcomes for such events. Time-sequenced AFM imagery following each annealing cycle has allowed us to assess the likelihood of a given outcome, such as the annihilation and/or propagation of defect pairs, depending on the local structure of the microphase-separated (and defect containing) environment. In essence, a disclination can change its core type by generating a dislocation. Dislocations play a crucial role in disclination propagation and annihilation. Two disclinations of the same core type, but with opposite signs, can annihilate while two disclinations of opposite core types and signs propagate. Interactions between pairs of paired disclinations have also been investigated. These events involve the reconfiguration of polymer chains through relinking or joining.

Finally, we have captured time-sequenced images taken after *ex situ* annealing treatments which give us a first glimpse of the intermediate ''transition state'' which mediates transformations from one defect environment to another. This process apparently involves ''necking'' in the vicinity of extant defect structures, driven by localized stress fields, which govern the downhill energy path of the system.

It is our belief that we are approaching a point where one should be able to accurately predict the dynamical evolution of microphase-separating ultrathin polymeric structures when subjected to thermal annealing. An understanding of topological defect evolution, when coupled with knowledge of the kinetics for polymer flow in contact with supporting

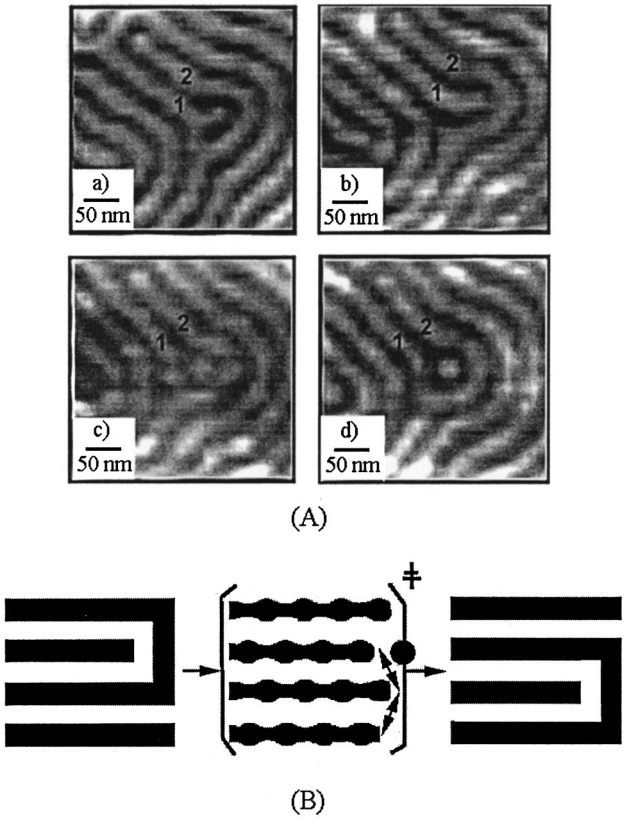

FIG. 10. (A) Time lapse AFM images, 300 nm×300 nm, showing the morphology changes in L thick domains between sequential annealing treatments (523 K, 1 h). PMMA (bright) microdomains in each image are numbered to easily identify them as they undergo ''necking'' where cylindrical domains in the vicinity of a defect form round, ball-like fragments in order to disconnect from the original microdomain and relink with neighboring microdomains. After further annealing, these round fragments relax back to cylinders. (B) Necking sketched schematically including an intermediate ''transitional state'' between two microdomain configurations. This illustrates the relinking of balled-up microdomains in the presence of defects. Arrows in the intermediate stage indicate where the new linking of microdomains occurs.

substrates, should allow us to predict and perhaps control the pathways by which thermal annealing occurs in technologically important films of these nanostructured materials.

ACKNOWLEDGMENTS

Discussions with Professors Heinrich Jaeger and Thomas Witten are gratefully acknowledged. This work was primarily supported by the NSF-Materials Research Science and Engineering Center at The University of Chicago, DMR-9808595. Further support is also acknowledged from the Air Force Office of Scientific Research.

[1] I. C. Sanchez, *Physics of Polymer Surfaces and Interfaces* (Butterworth–Heinemann, Boston, 1992).
[2] J. H. v. Zanten, W. E. Wallace, and W. L. Wu, Phys. Rev. E **53**, R2053 (1996).
[3] E. K. Lin, W. Wu, and S. K. Satija, Macromolecules **30**, 7224 (1997).
[4] X. Zheng, B. B. Sauer, J. G. V. Alsten *et al.*, Phys. Rev. Lett. **74**, 407 (1995).
[5] B. Frank, A. P. Gast, T. P. Russell *et al.*, Macromolecules **29**, 6531 (1996).
[6] P. F. Green, D. B. Adolf, and L. R. Gilliom, Macromolecules **24**, 3377 (1991).
[7] M. W. Hamersky, M. A. Hillmyer, M. Tirrell *et al.*, Macromolecules **31**, 5363 (1998).
[8] K. R. Shull, E. J. Kramer, F. S. Bates, and J. H. Rosedale, Macromolecules **24**, 1383 (1991).
[9] P. G. d. Gennes, *The Physics of Liquid Crystals* (Clarendon, Oxford, 1969).
[10] P. M. Chaikin and T. C. Lubensky, *Principles of Condensed Matter Physics* (Cambridge University Press, Cambridge, 1995), Chap. 9.
[11] R. Balian, M. Kleman, and J. P. Poirier, *Physics of Defects* (North–Holland, New York, 1980).
[12] K. Amundson, E. Helfand, S. S. Patel *et al.*, Macromolecules **25**, 1935 (1992).
[13] K. Amundson, E. Helfand, X. Quan, and S. D. Smith, Macromolecules **26**, 2698 (1993).
[14] K. Amundson and E. Helfand, Macromolecules **26**, 1324 (1993).
[15] K. Amundson, E. Helfand, X. Quan *et al.*, Macromolecules **27**, 6559 (1994).
[16] M. S. Turner, M. Maaloum, D. Ausserre *et al.*, J. Phys. II **4**, 689 (1994).
[17] E. Huang, P. Mansky, T. P. Russell *et al.*, Macromolecules **33**, 80 (2000).
[18] M. S. Turner, M. Maaloum, D. Ausserre *et al.*, J. Phys. II **4**, 689 (1994).
[19] S. P. Gido, J. Gunther, E. L. Thomas, and D. Hoffman, Macromolecules **26**, 4506 (1993).
[20] R. Ries, G. Lieser, S. Schwiegk, and G. Wegner, Acta Polym. **48**, 536 (1997).
[21] P. M. Wilson and D. C. Martin, Macromolecules **29**, 842 (1996).
[22] M. A. Singh, C. R. Harkless, S. E. Nagler *et al.*, Phys. Rev. B **47**, 8425 (1993).
[23] A. Karim, N. Singh, M. Sikka *et al.*, J. Chem. Phys. **100**, 1621 (1994).
[24] A. Menelle, T. P. Russell, S. H. Anastasiadis *et al.*, Phys. Rev. Lett. **68**, 67 (1992).
[25] B. D. Ratner and V. V. Tsukruk, *Scanning Probe Microscopy of Polymers* (ACS, Washington, D.C., 1998).
[26] J. Hahm, W. A. Lopes, H. M. Jaeger, and S. J. Sibener, J. Chem. Phys. **109**, 10111 (1998).
[27] J. Hahm and S. Sibener, Langmuir **16**, 4766 (2000).
[28] T. L. Morkved, W. A. Lopes, J. Hahm *et al.*, Polymer **39**, 3871 (1998).
[29] K. Y. Suh, Y. S. Kim, and H. H. Lee, J. Chem. Phys. **108**, 1253 (1998).
[30] D. Ausserre, D. Chatenay, G. Coulon, and B. Collin, J. Phys. (Paris) **51**, 2571 (1990).
[31] G. Coulon, B. Collin, D. Chatenay, and Y. Gallot, J. Phys. II **3**, 697 (1993).
[32] P. W. Voorhees, J. Stat. Phys. **38**, 231 (1985).
[33] J. D. Ferry, *Viscoelastic Properties of Polymers*, 3rd ed. (Wiley, New York, 1980).
[34] A. Casale, A. Mononi, and C. Civardi, Angew. Makromol. Chem. **53**, 277 (1971).
[35] A. Casale and R. S. Porter, J. Macromol. Sci. Rev. Macromol. Chem. C **5**, 387 (1971).
[36] S. Chandrasekhar, *Liquid Crystals* (Cambridge University Press, New York, 1977).
[37] K. Minoura, Y. Kimura, K. Ito, and R. Hayakawa, Mol. Cryst. Liq. Cryst. Sci. Technol., Sect. A **302**, 345 (1997).
[38] P. T. Mather, D. S. Pearson, and R. G. Larson, Liq. Cryst. **20**, 527 (1996).
[39] T. V. Kushnareva, S. V. Kushnarev, and V. K. Pershin, Crystallogr. Rep. **42**, 294 (1997).
[40] A. M. Sonnet and E. G. Virga, Phys. Rev. E **56**, 6834 (1997).
[41] W. Wang, T. Shiwaku, and T. Hashimoto, J. Chem. Phys. **108**, 1618 (1997).
[42] M. Kleman, *Points, Lines, and Walls* (Wiley, New York, 1983).
[43] G. Mazelet and M. Kleman, Polymer **27**, 714 (1986).